Exosome-Mediated mRNA Delivery For SARS-CoV-2 Vaccination

*Shang-Jui Tsai, *Chenxu Guo, ^Nadia A. Atai, and *Stephen J. Gould

* Department of Biological Chemistry, The Johns Hopkins University School of Medicine, 725 North Wolfe Street, Baltimore, MD, 21205

^ Capricor Therapeutics, Inc. 8840 Wilshire Blvd. 2nd Floor, Beverly Hills, CA 90211

Correspondence:

Name: Stephen J. Gould Ph.D

Address: 725 North Wolfe Street, Baltimore, MD 21205

Phone number: 443 847 9918

Email: sgould@jhmi.edu

Running title: Exosomal SARS-CoV-2 vaccine

Key Words: COVID19, spike, nucleocapsid, exosomes, mRNA, lipid, antibody, T-cell

Abstract

Background

In less than a year from its zoonotic entry into the human population, SARS-CoV-2 has infected more than 45 million people, caused 1.2 million deaths, and induced widespread societal disruption. Leading SARS-CoV-2 vaccine candidates immunize with the viral spike protein delivered on viral vectors, encoded by injected mRNAs, or as purified protein. Here we describe a different approach to SARS-CoV-2 vaccine development that uses exosomes to deliver mRNAs that encode antigens from multiple SARS-CoV-2 structural proteins.

Approach

Exosomes were purified and loaded with mRNAs designed to express (i) an artificial fusion protein, LSNME, that contains portions of the viral spike, nucleocapsid, membrane, and envelope proteins, and (ii) a functional form of spike. The resulting combinatorial vaccine, LSNME/S^{W1}, was injected into thirteen weeks-old, male C57BL/6J mice, followed by interrogation of humoral and cellular immune responses to the SARS-CoV-2 nucleocapsid and spike proteins, as well as hematological and histological analysis to interrogate animals for possible adverse effects.

Results

Immunized mice developed $CD4^+$, and $CD8^+$ T-cell reactivities that respond to both the SARS-CoV-2 nucelocapsid protein and the SARS-CoV-2 spike protein. These responses

were apparent nearly two months after the conclusion of vaccination, as expected for a durable response to vaccination. In addition, the spike-reactive CD4+ T-cells response was associated with elevated expression of interferon gamma, indicative of a Th1 response, and a lesser induction of interleukin 4, a Th2-associated cytokine. Vaccinated mice showed no sign of altered growth, injection-site hypersensitivity, change in white blood cell profiles, or alterations in organ morphology. Consistent with these results, we also detected moderate but sustained anti-nucleocapsid and anti-spike antibodies in the plasma of vaccinated animals.

Conclusion

Taken together, these results validate the use of exosomes for delivering functional mRNAs into target cells *in vitro* and *in vivo*, and more specifically, establish that the LSNME/S^{W1} vaccine induced broad immunity to multiple SARS-CoV-2 proteins.

Introduction

COVID-19 is caused by severe acute respiratory syndrome coronavirus 2 (SARS-CoV-2) (Coronaviridae Study Group of the International Committee on Taxonomy of, 2020; Zhou et al., 2020b). COVID-19 typically presents with symptoms common to many respiratory infections such as fever and cough (Gandhi et al., 2020) but can also progress to acute respiratory distress, disseminated disease, and death (Force et al., 2012; Guo et al., 2020; Richardson et al., 2020; Wang et al., 2020; Zhou et al., 2020a). Humans have long been host to several mildly pathogenic beta-coronaviruses (OC43, HKU1, etc. (Corman et al., 2018)) but SARS-CoV-2 entered the human population in late 2019 as the result of a zoonotic leap. SARS-CoV-2 is closely related to a pair of prior bat-to-human zoonoses that were responsible for the outbreaks of severe acute respiratory syndrome (SARS-CoV) in 2002 (Graham and Baric, 2010) and middle east respiratory syndrome (MERS-CoV) in 2012 (Memish et al., 2013). While SARS-CoV-2 infection is associated with lower mortality than SARS-CoV or MERS-CoV, SARS-CoV-2 displays a higher rate of transmission and has become a major cause of morbidity and mortality worldwide (https://www.cdc.gov/coronavirus/2019-ncov/hcp/clinical-guidance-management-patients.html)(coronavirus.jhu.edu)(Korber et al., 2020).

Infection of a cell by SARS-CoV-2 results in the translation of its viral genomic RNA (gRNA) into large polyproteins, open reading frame 1 (orf1a) and orf1ab, which are processed to release 16 nonstructural proteins (nsp1-16) (V'Kovski et al., 2020). These early proteins prime the host cell for virus replication and mediate the synthesis of subgenomic viral RNAs. These encode 12 additional proteins, including the SARS-CoV-

2 structural proteins Nucleocapsid (N), Spike (S), Membrane (M), and Envelope (E). The coronavirus integral membrane proteins S, M, and E are co-translationally translocated into the endoplasmic reticulum (ER) and trafficked by the secretory pathway to Golgi and Golgi-related compartments (Ruch and Machamer, 2012; Ujike and Taguchi, 2015), and perhaps other compartments of the cell as well (Ghosh et al., 2020). During their intracellular trafficking, the S, M, and E proteins work together to recruit N protein-gRNA complexes into nascent virions and to drive the budding of infectious vesicles from the host cell membrane. The resulting SARS-CoV-2 virions are small, membrane-bound vesicles of ~100 nm diameter, with large, spike-like trimers of S that protrude from the vesicle surface (Yao et al., 2020).

The S protein interacts with a variety of cell surface proteins including its canonical receptor, angiotensin-converting enzyme II (ACE2) (Hoffmann et al., 2020; Matheson and Lehner, 2020; Zhou et al., 2020b), and neuropilin-1 (Cantuti-Castelvetri et al., 2020; Daly et al., 2020). SARS-CoV-2 receptors and other infection mediators (e.g. TMPRSS2 (Hoffmann et al., 2020)) are expressed within the respiratory tract, consistent with its respiratory mode of transmission (Mason, 2020). However, the surface proteins that facilitate SARS-CoV-2 binding and entry are also expressed in many other cell types, allowing SARS-CoV-2 to spread within the body and impact multiple organ systems, including the brain, heart, gastrointestinal tract, circulatory system, and immune system (Cantuti-Castelvetri et al., 2020; Daly et al., 2020; Li et al., 2020; Nicin et al., 2020; Singh et al., 2020; Ziegler et al., 2020).

Studies show that COVID-19 patients generate potent cellular and humoral immune responses to the virus (Poland et al., 2020; St John and Rathore, 2020; Zost et al., 2020). Moreover, animal studies provide clear evidence that SARS-CoV-2 infection elicits immune responses that reverse the course of disease, clear the virus, and confer resistance to reinfection (Bosco-Lauth et al., 2020; Chandrashekar et al., 2020; Deng et al., 2020; Shan et al., 2020). Taken together, these observations augur well for control of SARS-CoV-2 transmission and disease through vaccination. Although to date there are no approved vaccines for any human coronavirus, disease-preventing vaccines have been progressively developed for multiple animal coronaviruses (Tizard, 2020). Most of these coronavirus vaccines are based on attenuated viruses, which elicit immune responses to all viral proteins, or inactivated virus particle vaccines, which induce immunity to the structural proteins of the virus (i.e. S, N, M, and E). Of the SARS-CoV-2 vaccines selected for rapid development, all are based on immunization with just a single viral protein, the large, spike-like S protein (Slaoui and Hepburn, 2020)(Samrat et al., 2020).

Although S-based SARS-CoV-2 vaccines all target the same protein, they vary significantly in antigen structure and mode of antigen delivery. Forms of S in vaccine trials range from S protein fragments (Walsh et al., 2020) to full-length forms of S (Bos et al., 2020; Graham et al., 2020; Hassan et al., 2020; Jackson et al., 2020; Keech et al., 2020; Walsh et al., 2020; Zhu et al., 2020) though none deliver the kinds of full-length, functional form of S encoded by SARS-CoV-2. As for the modes of S antigen delivery, most enlist host cells to express the S antigen component of their vaccine, from either injected

mRNAs (Jackson et al., 2020; Walsh et al., 2020) or infectious viral vectors (Bos et al., 2020; Graham et al., 2020; Hassan et al., 2020; Zhu et al., 2020) while some involve direct injection of purified, recombinant S protein (Keech et al., 2020). Here we describe an alternative approach to SARS-CoV-2 vaccination that combines the features of exosome-based mRNA delivery with the expression of viral antigens in forms designed for antigen presentation by major histocompatibility (MHC) Class I and Class II pathways(Imai et al., 2019). Exosomes are small extracellular vesicles (sEVs) of ~30-150 nm in diameter that are made by all cells, abundant in all biofluids, and mediate intercellular transmission of signals and macromolecules, including genetic information such as RNAs (Pegtel and Gould, 2019). Here we describe the results of a trial immunization study in which exosomes were used to deliver multiple mRNAs designed to express fragments of the S, N, M, and E proteins targeted to MHC Class I and Class II antigen processing compartment, as well as a full-length, functional form of S.

Results

Exosome-mRNA-directed protein expression

To develop a system for exosome-mediated mRNA delivery we first established a protocol for exosome purification from cultured human cells. Towards this end, 293F cells were grown in suspension in chemically-defined media, free of animal products and antibiotic supplements. Cells and cell debris were removed by centrifugation and filtration to generate a clarified tissue culture supernatant (CTCS), followed by purification of the CTCS by filtration and chromatography. This process yielded a population of small EVs that have the expected ultrastructure and size distribution profile of human exosomes and contain the exosomal marker proteins CD9 and CD63 (***Fig. 1***). This process concentrated exosomes ~500-fold, to ~2 x 10^{12} exosomes/mL, with an average recovery of 35%.

To determine whether the treatment of cells with exosome-mRNA formulations could induce cells to express these mRNAs, we synthesized an mRNA containing a codon-optimized open reading frame (ORF) for Antares2, a reporter protein comprised of the luciferase teLuc fused to two copies of the fluorescent protein CyOFP1 (CyOFP1-teLuc-CyOFP1) (Yeh et al., 2017). Antares2 expression can be measured via its luciferase activity (diphenylterazine-induced, bioluminescence resonance energy transfer (BRET)-mediated bioluminescence) or via its CyOFP1-mediated fluorescence (excitation range of 475nm-535 nm; emission range of 565nm-610nm). This mRNA was loaded into exosomes and then incubated with cultures of HEK293 cells overnight. The cells were then processed for Antares2 luciferase activity and fluorescence microscopy (***Fig. 2***).

Treated cells displayed high levels of Antares2 luciferase activity that was dependent on the specific order of component addition during the exosome formulation process. When interrogated by fluorescence microscopy, the cells displayed the expected expression of Antares2-mediated fluorescence.

Design and validation of SNME and S^{W1} mRNAs

To test whether exosome-mRNA formulations can elicit immune responses to proteins of SARS-CoV-2, we first synthesized a pair of mRNAs designed to express SARS-CoV-2 antigens. The first of these mRNAs encoded a membrane protein (LSNME) comprised of the receptor binding domain (RBD) of S, the entire N protein, and soluble portions of the M and E proteins, all expressed within the extracellular domain of the human Lamp1 protein. This protein is predicted to be degraded into peptides for antigen presentation by the MHC Class I system, and if expressed in antigen-presenting cells (APCs), to be degraded into peptides for antigen presentation by MHC Class II molecules (Gupta et al., 2006)(Imai et al., 2019). Expression of such a protein in a non-APC cell type such as HEK293 is expected to result in its accumulation in the ER, and consistent with this hypothesis, staining HEK293 cells transfected with this mRNA expressed with a COVID-19 patient plasma identified an ER-localized protein (***Fig. 3A, B***). The second of these *in vitro* synthesized mRNAs was designed to express the full-length, functional form of S from the original Wuhan-1 isolate of SARS-CoV-2 (S^{W1}) (Zhou et al., 2020b). Transfection of this mRNA into HEK293 cells led to expression of a distinct protein that was also recognized by antibodies present in a COVID-19 patient plasma (***Fig. 3C, D***). Taken

together, these results demonstrate that these mRNAs encode that are reactive with COVID-19 patient plasmas and have expected subcellular distributions.

The LSNME/S^{W1} vaccine induces antibody responses to N and S

A single exosome-mRNA formulation containing both the LSNME and S^{W1} mRNAs (hereafter referred to as the LSNME/S^{W1} vaccine) was injected (intramuscular) into 13 weeks-old male C57BL/6J mice (***Fig. 4***). The vaccine was dosed at 4 ug or 0.25 ug equivalents of each mRNA and injections were performed on day 1 (primary immunization), day 21 (1st boost), and day 42 (2nd boost). Blood (0.1 mL) was collected on days 14, 35, 56, 70 and 84. On day 84 the animals were sacrificed to obtain tissue samples for histological analysis and splenocytes for blood cell studies. Using ELISA kits adapted for the detection of mouse antibodies, we observed that vaccinated animals displayed a dose-dependent antibody response to both the SARS-CoV-2 N protein and S protein. These antibody reactions were not particularly robust but they were long-lasting, persisting to 7 weeks after the final boost with little evidence of decline. It should be noted that the modest antibody production was expected in the case of the N protein, as the LSNME mRNA is designed to stimulate cellular immune responses rather than the production of anti-N antibodies.

The LSNME/S^{W1} vaccine induces cellular immune responses to N and S

Vaccinated and control animals were also interrogated for the presence of antigen-reactive CD4+ and CD8+ T-cells. This was carried out by collecting splenocytes at the completion of the trial (day 84) using a CFSE proliferation assay in the presence or

absence of recombinant N and S proteins. These experiments revealed that vaccination had induced a significant increase in the percentages of $CD4^+$ T-cells and $CD8^+$ T-cells that proliferated in response to addition of either recombinant N protein or recombinant S protein to the culture media (***Fig. 5A-D***). These vaccine-specific, antigen-induced proliferative responses demonstrate that the LSNME/S^{W1} vaccine achieved its primary goal, which was to prime the cellular arm of the immune system to generate N-reactive $CD4^+$ and $CD8^+$ T-cells, and also S-reactive $CD4^+$ and $CD8^+$ T-cells. In additional experiments, we stained antigen-induced T-cells cells for the expression of interferon gamma (IFNγ) and interleukin 4 (IL4). These experiments revealed that the S-reactive $CD4^+$ T-cell population displayed elevated expression of the Th1-associated cytokine IFNγ, and to a lesser extent, the Th2-associated cytokine IL4 (***Fig 6***). In contrast, N-reactive T-cells failed to display an N-induced expression of either IFNγ or IL4.

Absence of vaccine-induced adverse reactions

Control and vaccinated animals were examined regularly for overall appearance, general behavior, and injection site inflammation (redness, swelling). No vaccine-related differences were observed in any of these variables, and animals from all groups displayed similar age-related increases in body mass (***supplemental figure 1***). Vaccination also had no discernable effect on blood cell counts (***supplemental figure 2***). Histological analyses were performed on all animals at the conclusion of the study by an independent histology service, which reported that vaccinated animals showed no difference in overall appearance of any of the tissues that were examined. Representative

images are presented for brain, lung, heart, liver, spleen, kidney, and side of injection skeletal muscle in an animal from each of the trial groups (***Fig. 7***).

Discussion

Exosomes represent a novel drug delivery vehicle capable of protecting labile cargoes from degradation and delivering them into the cytoplasm of target cells (Kamerkar et al., 2017; Li et al., 2017; O'Brien et al., 2020). This is particularly relevant for the development of RNA-based vaccines and therapeutics, as unprotected RNA-based drugs are subject to rapid turnover, poor targeting, and in some cases unwanted side effects arising from naked nucleic acid injection. Encapsulating RNAs in liposomes and other types of lipid nanoparticles (LNPs) is one approach to solving these problems (Witzigmann et al., 2020; Yu et al., 2020), but LNPs are known to pose risks of their own (Peer, 2012), and in some cases LNP-RNA drugs have been associated with severe adverse effects (Hong et al., 2020). In contrast, exosomes are continually released by all cells, are abundant components of human blood and all other biofluids (Coumans et al., 2017; Pegtel and Gould, 2019), and are therefore well-tolerated drug-delivery vehicles in human (Kamerkar et al., 2017; Li et al., 2017; O'Brien et al., 2020). In addition, exosomes play critical roles in the intercellular delivery of signals and macromolecules, including the functional delivery of mRNAs and other RNAs, making RNA-loaded exosomes an attractive candidate for clinical applications of RNA therapeutics (O'Brien et al., 2020; Ratajczak et al., 2006; Skog et al., 2008).

.

In the present report, we established that formulations of purified exosomes, in vitro-synthesized mRNAs, and polycationic lipids can mediate mRNA transport into human cells, and functional expression of mRNA-encoded protein products. This was established first for Antares2, a bioluminescent and fluorescent protein that served as a reporter

protein for interrogating the effect of exosome-mRNA formulation variables that affect exosome-mediated mRNA delivery. It was then extended to the functional delivery of mRNAs encoding membrane proteins, including the multi-antigen carrier protein LSNME and S^{W1}, a functional spike protein. Taken together, these results indicate that mRNAs delivered via exosome-mRNA formulations can support cargo protein synthesis, regardless of whether the protein is predicted to be synthesized on free cytosolic ribosomes (e.g. Antares2) or on membrane-bound ribosomes that mediate co-translational translocation of the protein into the endoplasmic reticulum (e.g. LSNME and S^{W1}).

We also explored the ability of an exosome-RNA formulation to drive functional mRNA expression *in vivo* by injecting an exosome complex containing the LSNME and S^{W1} mRNAs (LSNME/S^{W1}) into mice and monitoring immune responses to the SARS-CoV-2 N and S proteins. This vaccine was administered at relatively low doses of 4 μg mRNA equivalents and 0.25 μg mRNA equivalents in the absence of adjuvant. Injections were spaced at three-week intervals, and blood samples were collected over the course of 12 weeks. The animals were then sacrificed and tissues were harvested for analysis of cellular immune responses and organ histology. Consistent with the goal of vaccine-induced development of balanced T-cell responses, vaccinated animals displayed antigen-induced proliferation of $CD4^+$ and $CD8^+$ T-cell responses to both the N and S proteins. These antigen-responsive CD4+ and CD8+ populations were present nearly two months after the final boost injection, indicating that LSNME/S^{W1} vaccination had elicited a sustained cellular immune response to both of these SARS-CoV-2 structural proteins.

Furthermore, when these cell populations were interrogated for antigen-induced expression of the cytokines IFNγ and IL4, we detected elevated expression of IFNγ in CD4+ T-cells exposed to exogenous S protein, as well as a more modest S-induced expression of IL4. These results raise the possibility that the LSNME/S^{W1} induces the kind of Th1-skewed cellular response desired for vaccine-induced immunity. These results are consistent with the design of the LSNME open reading frame, which is engineered to drive antigen processing by the MHC Class I and Class II pathways (Gupta et al., 2006; Imai et al., 2019; Wu et al., 1995). Vaccinated animals also developed durable antibody responses to the N and the S proteins. While the titers of these antibody responses were modest, they were sustained at relatively constant levels over the 7 weeks following the final boost injection. The relative strength of these immune responses is likely a consequence of the low mRNA dose of the LSNME/S^{W1} vaccine, and is likely to be amplified significantly by the >20-fold increase in dose projected in large animal models and human trials.

In conclusion, the results presented in this study validate the use of exosome-mRNA formulations for functional delivery of mRNAs both in cultured cells and in live animals. The successful use of exosomes to deliver Antares2 mRNA opens the door to follow-on studies aimed at optimizing exosome-RNA formulation conditions, as well as for characterizing the time-dependence of Antares2 expression, biodistribution of exosome-mediated RNA expression, injection site effects, and exosome-mediated tissue. As for the future development of the LSNME/S^{W1} vaccine, we anticipate that follow-on studies in larger animal models at doses comparable to other mRNA vaccines will demonstrate

a desirable combination of safety, balanced immune responses, and when challenged, protection against SARS-CoV-2 infection and/or disease.

Materials and Methods

Cell culture

293F cells (Gibco, Cat.# 51-0029) were tested for pathogens and found to be free of viral (cytomegalovirus, human immunodeficiency virus I and II, Epstein Barr virus, hepatitis B virus, and parvovirus B19), and bacterial (*Mycoplasma*) contaminants. Cells were maintained in FreeStyle 293 Expression Medium (Gibco, #12338-018) and incubated at 37°C in 8% CO_2. For exosome production, 293F cells were seeded at a density of 1.5 x 10^6 cells/ml in shaker flasks in a volume of ~1/4 the flask volume and grown at a shaking speed of 110 rpm. HEK293 cells were grown in Dulbecco's modified Eagle's medium supplemented with 10% fetal calf serum.

Exosome purification

293F cells were grown in shaker cultures for a period of three days. Cells and large cell debris were removed by centrifugation at 300 x *g* for 5 minutes followed by 3000 x *g* for 15 minutes. The resulting supernatant was passed through a 0.22 µm sterile filtration filter unit (Thermo Fisher, #566-0020) to generate a clarified tissue culture supernatant (CTCS). The CTCS was concentrated by centrifugal filtration (Centricon Plus-70, Ultracel-PL Membrane, 100 kDa size exclusion, Millipore Sigma # UFC710008), with ~120 mLs CTCS concentrated to ~0.5 mLs. Concentrated CTCS was then purified by size exclusion chromatography (SEC) in 1x PBS (qEV original columns/35 nm: Izon Science, #SP5), with the exosomes present in each 0.5 mL starting sample eluting in three 0.5 mL

fractions. Purified exosomes were reconcentrated using Amicon® Ultra-4 100 kDa cutoff spin columns (#UFC810024).

Nanoparticle Tracking Analysis (NTA)

Vesicle concentrations and size distribution profiles of exosome preparations were measured by nanoparticle tracking analysis (NTA) using a NanoSight NS300 (Malvern Panalytical, United Kingdom) in 1x PBS clarified by filtration through a 0.22 μm sterile filtration unit. Measurements were carried out in triplicates at ambient temperature with fixed camera settings (level of 14, screen gain of 10, detection threshold 3, and temperature of 21.7-22.2 °C).

Immunoblots

Exosome and cell lysates were separated by SDS-PAGE using pre-cast, 4-15% gradient gels (Bio-Rad 4561086) and transferred to PVDF membranes (ThermoFisher, #88518). Membranes were probed using antibodies directed against CD9, CD63 (System Biosciences EXOAB-CD9A-1 and EXOAB-CD63A-1, respectively), and actin (Sigma A2066), with HRP-conjugated goat anti-rabbit secondary antibody used for detection (Cell Signaling, #7074). Target proteins were visualized by chemiluminescence, and images were captured using a ChemiDoc imager (Bio-Rad).

Electron Microscopy

Exosomes were fixed by addition of formaldehyde to a final concentration of 4%. Carbon-coated grids were placed on top of a drop of the exosome suspension. Next, grids were

placed directly on top of a drop of 2% uranyl acetate. The resulting samples were examined with a Tecnai-12 G2 Spirit Biotwin transmission electron microscope (John Hopkins University, USA).

RNA loading

mRNAs were purified using RNeasy columns (Qiagen) and reuspended in DNase-free, RNase-free water using nuclease-free tips and tubes. RNAs were then combined with different combinations and amounts of polycationic lipids and exosomes, as well as in different orders of addition. RNA loading of exosomes for vaccine formulation involved pre-mixing of mRNAs with polycationic lipids followed by addition of exosomes.

Luciferase measurements and light microscopy

HEK293 cells were incubated with exosome-mRNA formulations overnight under standard culture conditions. Antares2 luciferase activity was measured by Live cell bioluminescence was collected after incubating with substrate diphenylterazine (MCE, HY-111382) at final concentration of 50 μM for 3 minutes. Readings were collected using a SpectraMax i3x (Molecular Devices). Fluorescence micrographs of Antares2 expression in transfected HEK293 cells were captured as PNG files using an EVOS M7000 microscope equipped with an Olympus UPlanSAPo 40x/0.95 objective.

Immunization

RNA-loaded exosome formulations were generated and then stored for 24 hours at 4˚C prior to injection of mice. Injection doses were at either 4 μg equivalents of each mRNA, or 0.25 μg equivalents of each mRNA. Immunizations were initiated on thirteen weeks-old, male C57BL/6J mice (Jackson Laboratory) housed under pathogen-free conditions at the Cedars-Sinai Medical Center animal facility. All animal experimentation was performed following institutional guidelines for animal care and were approved by the Cedars-Sinai Medical Center IACUC (#8602). All injections were at a volume of 50 μls.

Blood and tissue collection

Blood (~0.1 mL) was collected periodically from the orbital vein. At day 84, mice were deeply anesthetized using isoflurane, euthanized by cervical dislocation, and processed using standard surgical procedures to obtain spleen, lung, brain, heart, liver, kidney, muscle, and other tissues. Spleens were processed for splenocyte analysis, and all tissues were processed for histological analysis by fixation in 10% neutral buffered formalin. Histological analysis was performed by the service arm of the HIC/Comparative Pathology Program of the University of Washington.

ELISA for SARS-CoV-2 antigen-specific antibody responses

Mouse IgG antibody production against SARS-CoV-2 antigens was measured by enzyme-linked immunosorbent assays (ELISA). For antigens S1 (RBD) and N, pre-coated ELISA plates from RayBiotech were utilized (IEQ-CoV S RBD-IgG; IEQ-CoVN-IgG), and the experiments were performed according to the manufacturer's instructions,

with modification. Briefly, mouse plasmas at dilutions of 1:50 were added to antigen pre-coated wells in duplicates and incubated at room temperature (RT) for 2 hours on a shaker (200 rpm). The plates were washed 4 times with wash buffer followed by blocking for 2 hours at RT with 1% BSA in PBS. Mouse antibodies bound to the antigens coated on the ELISA plates were detected using HRP-conjugated goat anti-mouse secondary antibodies (Jackson Immuno Research Inc.) Plates were washed 4 times with washing buffer, and developed using TMB substrate (RayBiotech). Microplate Reader was used to measure the absorbance at 650 nm (SpectraMaxID3, Molecular Devices, with SoftMax Pro7 software).

Single cell splenocyte preparation

After terminal blood collection mice were euthanized, and part of fresh spleens were harvested. Single cell splenocyte preparation was obtained by machinal passage through a 40 µm nylon cell strainer (BD Falcon, #352340). Erythrocytes were depleted using Ammonium-Chloride-Potassium (ACK) lysis buffer (Gibco, #A10492-01), and splenocytes were washed using R10 media by centrifuging at 300x *g* for 5 minutes at RT. R10 media (RPMI 1640 media (ATCC, Cat#302001) supplemented with 10% fetal bovine serum (FBS) (Atlas, #E01C17A1), 50 µM 2-mercaptoethanol (Gibco, #21985-023), penicillin/streptomycin (VWR life sciences, #K952), and 10 mM HEPES(Gibco, #15630-080)) was used for all analyses of blood cells. The cells were resuspended in fresh media and counted in hemocytometer counting chamber to be used in subsequent experiments.

Spleen lymphocyte population characterization

Splenocytes (2 x 10^5 cells/mouse) were resuspended in 100 µL of 10% FBS in 1x PBS and incubated with fluorochrome-conjugated antibodies for surface staining of CD3 (Invitrogen, #17-0032-82) CD4 (Biolegend, #100433), CD8 (Biolegend, #100708), B220 (BD, #552771) CD11c (Invitrogen, #17-0114-81), F4/80 (Invitrogen, #MF48004) Ly6G (Invitrogen, #11-9668-80) and Ly6C (BD, #560592)) for 30 minutes at 4 ˚C in the dark. Following incubation, samples were washed twice with 200 µLs 10% FBS in 1x PBS and centrifuged at 300 x *g* for 5 minutes at RT to remove unbound antibodies. Next the cells were fixed with 100 µLs ICS fixation buffer (Invitrogen, #00-8222-49). Samples were analyzed on a FACS Canto II (BD Biosciences) with 2,000 – 10,000 recorded lymphocytes . The data analysis was performed using FlowJo 10 software (FlowJo, LLC) and presented as a percentage change in the immune cell population compared to the vehicle-treated group.

SARS-CoV-2 antigen-specific T cell proliferation assay using CFSE

Splenocytes were resuspended at 10^6 cells/mL in 10% FBS in 1xPBS and stained with carboxyfluorescein succinimidyl ester (CFSE) (Invitrogen, #C34554) by rapidly mixing equal volume of cell suspension with 10 µM CFSE in 10% FBS in 1x PBS for 5 minutes at 37°C. The labeled cells were washed three times with R10 complete medium. The cells were incubated for 96 hours in the presence of 10 µg/mL SARS-CoV-2 antigens N or S1 (Acro Biosystems, #NUN-C5227; SIN-C52H4) or medium alone as negative control. After 96 hours, cells were washed with 200 µLs 10% FBS in 1xPBS and centrifuged at 300 x *g* for 5 minutes at RT. Cells were then stained with anti-CD3-APC (Invitrogen, #17-0032-82), anti-CD4-PerCP-Cy5.5 (Biolegend, #100433), and anti-CD8-PE antibodies

(Biolegend, #MCD0801) for 30 minutes at 4˚C. The stained cells were washed twice with 200 µLs 1x PBS and analyzed on a FACS Canto II (BD Biosciences). For analysis, lymphocytes were first gated for CD3+ T-cells, then for CD4+/CD8− or CD8+/CD4− populations. The data analysis was performed using FlowJo 10 software (FlowJo LLC).

Intracellular staining for cytokines

2.0 x 10^5 splenocytes/mouse were incubated for 72 hours in the presence of 10 µg/mL SARs-CoV2 antigens N or S1 (Acro Biosystems) or R10 medium alone (negative control). After 72 hours, the cells were washed with fresh R10 medium and incubated with phorbol myristate acetate (PMA) at concentration of 50 ng/mL (Sigma, #P1585), ionomycin at concentration of 350 ng/mL (Invitrogen, #124222), and GogiPlug at concentration of 0.8 µL/mL (Invitrogen, #51-2301KZ) for 4 hours to amplify cytokine expression in T cells. The cells were then washed with 10% FBS in 1x PBS and stained with anti-CD3-APC, anti-CD4-PerCP-Cy5.5, and anti-CD8-PE antibodies (Added above) for 30 minutes at 4˚C in dark. The cells were washed twice with 1xPBS followed by permeabilization step using ready-to-use buffer (Invitrogen #00-8333-56). Next the cells were fixed with ICS fixation bufferAdded above for 10 minutes at RT in dark and stained intracellular for IFN-γ (eBioscience, #11-7311-82), IL-10 (eBioscience, #11-7101-82), IL-4 (Invitrogen, #12-7041-41) and Foxp3 (Invitrogen, #12-5773-80) overnight at 4˚C in permeabilization buffer. The stained cells were analyzed on a BD FACS Canto II with 5,000 – 10,000 recorded lymphocytes. The data analysis was performed using FlowJo 10 software.

Statistical Analysis

Statistical analysis was performed using GraphPad Prism 8 software for Windows/Mac (GraphPad Software, La Jolla California USA). Results were reported as mean ± standard deviation or mean ± standard error, differences were analyzed using Student's t-test and one-way analysis of variance.

Sources of Support: This study was conducted with support from Capricor and from Johns Hopkins University.

Disclosures: S.J.G is a paid consultant for Capricor, holds equity in Capricor, and is co-inventor of intellectual property licensed by Capricor. S.J.T. is co-inventor of intellectual property licensed by Capricor. C.G. is co-inventor of intellectual property licensed by Capricor. N.A. is an employee of Capricor.

Acknowledgments: We thank Omid Sheikh, Connie Landaverde, Alanna Sedgwick, Justin Nice, and Saravana Kanagavelu for outstanding technical assistance during the course of these studies.

Figure Legends

Figure 1. Exosome purification and characterization. (A) Schematic of the exosome purification process. (B) NTA analysis of purified exosomes showing a mean exosome diameter of ~115 nm. (C) Negative stain electron microscopic analysis of purified exosomes, showing two vesicles with the expected size ranges of human exosomes. Bar, 100 nm. (D) Immunoblot analysis of cell and exosome lysates probed using antibodies for CD9, CD63 and actin.

Figure 2. Antares2 expression levels in cells following treatment with exosome-mRNA formulations. (A) Mean luciferase activities (+/- standard error of the mean) of cells treated with different exosome-mRNA formulations. Cells were treated with formulations in which (brown) mRNA and lipid (LFN) were mixed prior to exosome loading, (orange) exosomes and mRNA were mixed prior to lipid addition, (grey) exosomes and lipid were mixed prior to addition of mRNA, and (black) mRNA alone was added. (B, C) Light micrographs of HEK293 cells treated with the formulation in which mRNA and lipid were mixed prior to exosome loading (B) fluorescence microscopy showing exosome mRNA induced Antares2 fluorescence and (C) merged fluorescence and transmission light microscopy showing the cell-to-cell variability in Antares2 expression. Bar, 75 µm.

Figure 3. Expression of S^{W1} and LSNME following mRNA transfection. (A, B) Fluorescence micrographs of HEK293 cells stained with DAPI and a plasma from a COVID-19 patient. (C-F) Fluorescence micrographs of HEK293 cells stained with DAPI

and plasmas from a COVID-19 patient following their transfection with the (C, D) S^{W1}-encoding mRNA and (E, F) the LSNME-encoding mRNA. Bar, 50 µm.

Figure 4. LSNME/S^{W1} vaccination induces antibody responses to SARS-CoV-2 N and S protein. (A) Schematic of immunization and blood/tissue collection timeline. (B) Anti-N ELISA results of diluted plasma from (grey bars and black circles) individual six control mice, (orange bars and black squares) six mice immunized with 0.25 µg equivalents of each mRNA, and (rust bars and black triangles) six mice immunized with 4 µg equivalents of each mRNA. (C) Anti-S1 ELISA results of diluted plasma from (grey bars and black circles) individual six control mice, (orange bars and black squares) six mice immunized with 0.25 µg equivalents of each mRNA, and (rust bars and black triangles) six mice immunized with 4 µg equivalents of each mRNA. Height of bars represents the mean, error bars represent +/- one standard error of the mean, and the statistical significance of differences between different groups is reflected in Student's t-test values of * for <0.05, ** for <0.005, and *** for <0.0005.

Figure 5. LSNME/S^{W1} vaccination induces $CD4^+$ and $CD8^+$ T-cell responses. CFSE-labeled splenocytes were interrogated by flow cytometry following incubation in the absence or presence of (A, B) purified, recombinant N protein or (C, D) purified, recombinant S protein, and for antibodies specific for CD4 and CD8. Differences in proliferation of $CD4^+$ cells and $CD8^+$ cells were plotted for (grey bars and black circles) individual six control mice, (orange bars and black squares) six mice immunized with 0.25 µg equivalents of each mRNA, and (rust bars and black triangles) six mice immunized

with 4 μg equivalents of each mRNA. Height of bars represents the mean, error bars represent +/- one standard error of the mean, and the statistical significance of differences between different groups is reflected in Student's t-test values of * for <0.05 and ** for <0.005.

Figure 6. LSNME/S^{W1} vaccination leads to S-induced expression of IFNγ and IL4 by CD4^{+} T-cells. Splenocytes were interrogated by flow cytometry following incubation in the absence or presence of (A, B) purified, recombinant N protein or (C, D) purified, recombinant S protein, and labeling with antibodies specific for CD4 or CD8, and for IFNγ or IL4. Differences in labeling for IFNγ or IL4 in CD4^{+} CD8^{+} cell populations were plotted for (grey bars and black circles) individual six control mice, (orange bars and black squares) six mice immunized with 0.25 μg equivalents of each mRNA, and (rust bars and black triangles) six mice immunized with 4 μg equivalents of each mRNA. Height of bars represents the mean, error bars represent +/- one standard error of the mean, and the statistical significance of differences between different groups is reflected in Student's t-test values of * for <0.05.

Figure 7. Absence of tissue pathology upon LSNME/S^{W1} vaccination. Representative micrographs from histological analysis (hematoxylin and eosin stain) of lung, brain, heart, liver, kidney, spleen, and muscle (side of injection) of animals from (upper row) control mice, (middle row) mice immunized with the lower dose of the LSNME/S^{W1} vaccine, and (lower row) mice immunized with the higher dose of the LSNME/S^{W1} vaccine.

Supplemental Figure 1. Equivalent growth of vaccinated and control animals. Body mass of all mice was measured over the course of the study and plotted as average +/- the standard error of the mean, relative to the body mass at the initiation of the trial, with groups reported as (grey lines and circles) control mice, (orange lines and squares) lower dose-treated mice, and (rust lines and triangles) higher dose-treated mice.

Supplemental Figure 2. Vaccination does not induce changes in the proportional representation of key blood cell populations. Splenocytes were interrogated by flow cytometry using antibodies specific for (A) B220, (B) Ly6C, (C) CD11c, and (D) CD3. $CD3^+$ cells were further differentiated by staining for (E) CD4 and (F) CD8. No statistically significant differences were detected in these subpopulations of white blood cells.

References

Bos, R., Rutten, L., van der Lubbe, J.E.M., Bakkers, M.J.G., Hardenberg, G., Wegmann, F., Zuijdgeest, D., de Wilde, A.H., Koornneef, A., Verwilligen, A.*, et al.* (2020). Ad26 vector-based COVID-19 vaccine encoding a prefusion-stabilized SARS-CoV-2 Spike immunogen induces potent humoral and cellular immune responses. NPJ Vaccines *5*, 91.

Bosco-Lauth, A.M., Hartwig, A.E., Porter, S.M., Gordy, P.W., Nehring, M., Byas, A.D., VandeWoude, S., Ragan, I.K., Maison, R.M., and Bowen, R.A. (2020). Experimental infection of domestic dogs and cats with SARS-CoV-2: Pathogenesis, transmission, and response to reexposure in cats. Proc Natl Acad Sci U S A *117*, 26382-26388.

Cantuti-Castelvetri, L., Ojha, R., Pedro, L.D., Djannatian, M., Franz, J., Kuivanen, S., van der Meer, F., Kallio, K., Kaya, T., Anastasina, M.*, et al.* (2020). Neuropilin-1 facilitates SARS-CoV-2 cell entry and infectivity. Science. DOI: 10.1126/science.abd2985

Chandrashekar, A., Liu, J., Martinot, A.J., McMahan, K., Mercado, N.B., Peter, L., Tostanoski, L.H., Yu, J., Maliga, Z., Nekorchuk, M.*, et al.* (2020). SARS-CoV-2 infection protects against rechallenge in rhesus macaques. Science *369*, 812-817.

Corman, V.M., Muth, D., Niemeyer, D., and Drosten, C. (2018). Hosts and Sources of Endemic Human Coronaviruses. Adv Virus Res *100*, 163-188.

Coronaviridae Study Group of the International Committee on Taxonomy of, V. (2020). The species Severe acute respiratory syndrome-related coronavirus: classifying 2019-nCoV and naming it SARS-CoV-2. Nat Microbiol *5*, 536-544.

Coumans, F.A.W., Brisson, A.R., Buzas, E.I., Dignat-George, F., Drees, E.E.E., El-Andaloussi, S., Emanueli, C., Gasecka, A., Hendrix, A., Hill, A.F.*, et al.* (2017). Methodological Guidelines to Study Extracellular Vesicles. Circ Res *120*, 1632-1648.

Daly, J.L., Simonetti, B., Klein, K., Chen, K.E., Williamson, M.K., Anton-Plagaro, C., Shoemark, D.K., Simon-Gracia, L., Bauer, M., Hollandi, R.*, et al.* (2020). Neuropilin-1 is a host factor for SARS-CoV-2 infection. Science.

Deng, W., Bao, L., Liu, J., Xiao, C., Liu, J., Xue, J., Lv, Q., Qi, F., Gao, H., Yu, P.*, et al.* (2020). Primary exposure to SARS-CoV-2 protects against reinfection in rhesus macaques. Science *369*, 818-823.

Force, A.D.T., Ranieri, V.M., Rubenfeld, G.D., Thompson, B.T., Ferguson, N.D., Caldwell, E., Fan, E., Camporota, L., and Slutsky, A.S. (2012). Acute respiratory distress syndrome: the Berlin Definition. JAMA *307*, 2526-2533.

Gandhi, R.T., Lynch, J.B., and Del Rio, C. (2020). Mild or Moderate Covid-19. N Engl J Med *383*, 1757-1766.

Graham, R.L., and Baric, R.S. (2010). Recombination, reservoirs, and the modular spike: mechanisms of coronavirus cross-species transmission. J Virol *84*, 3134-3146.

Graham, S.P., McLean, R.K., Spencer, A.J., Belij-Rammerstorfer, S., Wright, D., Ulaszewska, M., Edwards, J.C., Hayes, J.W.P., Martini, V., Thakur, N.*, et al.* (2020). Evaluation of the immunogenicity of prime-boost vaccination with the replication-deficient viral vectored COVID-19 vaccine candidate ChAdOx1 nCoV-19. NPJ Vaccines *5*, 69.

Guo, T., Fan, Y., Chen, M., Wu, X., Zhang, L., He, T., Wang, H., Wan, J., Wang, X., and Lu, Z. (2020). Cardiovascular Implications of Fatal Outcomes of Patients With Coronavirus Disease 2019 (COVID-19). JAMA Cardiol *5*, 811-818.

Gupta, V., Tabiin, T.M., Sun, K., Chandrasekaran, A., Anwar, A., Yang, K., Chikhlikar, P., Salmon, J., Brusic, V., Marques, E.T.*, et al.* (2006). SARS coronavirus nucleocapsid immunodominant T-cell epitope cluster is common to both exogenous recombinant and endogenous DNA-encoded immunogens. Virology *347*, 127-139.

Hassan, A.O., Kafai, N.M., Dmitriev, I.P., Fox, J.M., Smith, B.K., Harvey, I.B., Chen, R.E., Winkler, E.S., Wessel, A.W., Case, J.B.*, et al.* (2020). A Single-Dose Intranasal ChAd Vaccine Protects Upper and Lower Respiratory Tracts against SARS-CoV-2. Cell *183*, 169-184 e113.

Hoffmann, M., Kleine-Weber, H., Schroeder, S., Kruger, N., Herrler, T., Erichsen, S., Schiergens, T.S., Herrler, G., Wu, N.H., Nitsche, A.*, et al.* (2020). SARS-CoV-2 Cell Entry Depends on ACE2 and TMPRSS2 and Is Blocked by a Clinically Proven Protease Inhibitor. Cell *181*, 271-280 e278.

Hong, D.S., Kang, Y.K., Borad, M., Sachdev, J., Ejadi, S., Lim, H.Y., Brenner, A.J., Park, K., Lee, J.L., Kim, T.Y.*, et al.* (2020). Phase 1 study of MRX34, a liposomal miR-34a mimic, in patients with advanced solid tumours. Br J Cancer *122*, 1630-1637.

Imai, J., Otani, M., and Sakai, T. (2019). Distinct Subcellular Compartments of Dendritic Cells Used for Cross-Presentation. Int J Mol Sci *20*.

Jackson, L.A., Anderson, E.J., Rouphael, N.G., Roberts, P.C., Makhene, M., Coler, R.N., McCullough, M.P., Chappell, J.D., Denison, M.R., Stevens, L.J.*, et al.* (2020). An mRNA Vaccine against SARS-CoV-2 - Preliminary Report. N Engl J Med.

Kamerkar, S., LeBleu, V.S., Sugimoto, H., Yang, S., Ruivo, C.F., Melo, S.A., Lee, J.J., and Kalluri, R. (2017). Exosomes facilitate therapeutic targeting of oncogenic KRAS in pancreatic cancer. Nature *546*, 498-503.

Keech, C., Albert, G., Cho, I., Robertson, A., Reed, P., Neal, S., Plested, J.S., Zhu, M., Cloney-Clark, S., Zhou, H.*, et al.* (2020). Phase 1-2 Trial of a SARS-CoV-2 Recombinant Spike Protein Nanoparticle Vaccine. N Engl J Med.

Korber, B., Fischer, W.M., Gnanakaran, S., Yoon, H., Theiler, J., Abfalterer, W., Hengartner, N., Giorgi, E.E., Bhattacharya, T., Foley, B.*, et al.* (2020). Tracking Changes in SARS-CoV-2 Spike: Evidence that D614G Increases Infectivity of the COVID-19 Virus. Cell *182*, 812-827 e819.

Li, L., Piontek, K., Ishida, M., Fausther, M., Dranoff, J.A., Fu, R., Mezey, E., Gould, S.J., Fordjour, F.K., Meltzer, S.J.*, et al.* (2017). Extracellular vesicles carry microRNA-195 to intrahepatic cholangiocarcinoma and improve survival in a rat model. Hepatology *65*, 501-514.

Li, M.Y., Li, L., Zhang, Y., and Wang, X.S. (2020). Expression of the SARS-CoV-2 cell receptor gene ACE2 in a wide variety of human tissues. Infect Dis Poverty *9*, 45.

Mason, R.J. (2020). Thoughts on the alveolar phase of COVID-19. Am J Physiol Lung Cell Mol Physiol *319*, L115-L120.

Matheson, N.J., and Lehner, P.J. (2020). How does SARS-CoV-2 cause COVID-19? Science *369*, 510-511.

Nicin, L., Abplanalp, W.T., Mellentin, H., Kattih, B., Tombor, L., John, D., Schmitto, J.D., Heineke, J., Emrich, F., Arsalan, M.*, et al.* (2020). Cell type-specific expression of the putative SARS-CoV-2 receptor ACE2 in human hearts. Eur Heart J *41*, 1804-1806.

O'Brien, K., Breyne, K., Ughetto, S., Laurent, L.C., and Breakefield, X.O. (2020). RNA delivery by extracellular vesicles in mammalian cells and its applications. Nat Rev Mol Cell Biol *21*, 585-606.

Peer, D. (2012). Immunotoxicity derived from manipulating leukocytes with lipid-based nanoparticles. Adv Drug Deliv Rev *64*, 1738-1748.

Pegtel, D.M., and Gould, S.J. (2019). Exosomes. Annu Rev Biochem *88*, 487-514.

Poland, G.A., Ovsyannikova, I.G., and Kennedy, R.B. (2020). SARS-CoV-2 immunity: review and applications to phase 3 vaccine candidates. Lancet.

Ratajczak, J., Miekus, K., Kucia, M., Zhang, J., Reca, R., Dvorak, P., and Ratajczak, M.Z. (2006). Embryonic stem cell-derived microvesicles reprogram hematopoietic progenitors: evidence for horizontal transfer of mRNA and protein delivery. Leukemia *20*, 847-856.

Richardson, S., Hirsch, J.S., Narasimhan, M., Crawford, J.M., McGinn, T., Davidson, K.W., the Northwell, C.-R.C., Barnaby, D.P., Becker, L.B., Chelico, J.D.*, et al.* (2020). Presenting Characteristics, Comorbidities, and Outcomes Among 5700 Patients Hospitalized With COVID-19 in the New York City Area. JAMA *323*, 2052-2059.

Ruch, T.R., and Machamer, C.E. (2012). The coronavirus E protein: assembly and beyond. Viruses *4*, 363-382.

Samrat, S.K., Tharappel, A.M., Li, Z., and Li, H. (2020). Prospect of SARS-CoV-2 spike protein: Potential role in vaccine and therapeutic development. Virus Res *288*, 198141.

Shan, C., Yao, Y.F., Yang, X.L., Zhou, Y.W., Gao, G., Peng, Y., Yang, L., Hu, X., Xiong, J., Jiang, R.D.*, et al.* (2020). Infection with novel coronavirus (SARS-CoV-2) causes pneumonia in Rhesus macaques. Cell Res *30*, 670-677.

Singh, M., Bansal, V., and Feschotte, C. (2020). A Single-Cell RNA Expression Map of Human Coronavirus Entry Factors. Cell Rep *32*, 108175.

Skog, J., Wurdinger, T., van Rijn, S., Meijer, D.H., Gainche, L., Sena-Esteves, M., Curry, W.T., Jr., Carter, B.S., Krichevsky, A.M., and Breakefield, X.O. (2008). Glioblastoma microvesicles transport RNA and proteins that promote tumour growth and provide diagnostic biomarkers. Nat Cell Biol *10*, 1470-1476.

Slaoui, M., and Hepburn, M. (2020). Developing Safe and Effective Covid Vaccines - Operation Warp Speed's Strategy and Approach. N Engl J Med *383*, 1701-1703.

St John, A.L., and Rathore, A.P.S. (2020). Early Insights into Immune Responses during COVID-19. J Immunol *205*, 555-564.

Tizard, I.R. (2020). Vaccination against coronaviruses in domestic animals. Vaccine *38*, 5123-5130.

Ujike, M., and Taguchi, F. (2015). Incorporation of spike and membrane glycoproteins into coronavirus virions. Viruses *7*, 1700-1725.

V'Kovski, P., Kratzel, A., Steiner, S., Stalder, H., and Thiel, V. (2020). Coronavirus biology and replication: implications for SARS-CoV-2. Nat Rev Microbiol.

Walsh, E.E., Frenck, R.W., Jr., Falsey, A.R., Kitchin, N., Absalon, J., Gurtman, A., Lockhart, S., Neuzil, K., Mulligan, M.J., Bailey, R.*, et al.* (2020). Safety and Immunogenicity of Two RNA-Based Covid-19 Vaccine Candidates. N Engl J Med.

Wang, D., Hu, B., Hu, C., Zhu, F., Liu, X., Zhang, J., Wang, B., Xiang, H., Cheng, Z., Xiong, Y.*, et al.* (2020). Clinical Characteristics of 138 Hospitalized Patients With 2019 Novel Coronavirus-Infected Pneumonia in Wuhan, China. JAMA *323*, 1061-1069.

Witzigmann, D., Kulkarni, J.A., Leung, J., Chen, S., Cullis, P.R., and van der Meel, R. (2020). Lipid nanoparticle technology for therapeutic gene regulation in the liver. Adv Drug Deliv Rev.

Wu, T.C., Guarnieri, F.G., Staveley-O'Carroll, K.F., Viscidi, R.P., Levitsky, H.I., Hedrick, L., Cho, K.R., August, J.T., and Pardoll, D.M. (1995). Engineering an intracellular pathway for major histocompatibility complex class II presentation of antigens. Proc Natl Acad Sci U S A *92*, 11671-11675.

Yao, H., Song, Y., Chen, Y., Wu, N., Xu, J., Sun, C., Zhang, J., Weng, T., Zhang, Z., Wu, Z*., et al.* (2020). Molecular Architecture of the SARS-CoV-2 Virus. Cell *183*, 730-738 e713.

Yeh, H.W., Karmach, O., Ji, A., Carter, D., Martins-Green, M.M., and Ai, H.W. (2017). Red-shifted luciferase-luciferin pairs for enhanced bioluminescence imaging. Nat Methods *14*, 971-974.

Yu, A.M., Choi, Y.H., and Tu, M.J. (2020). RNA Drugs and RNA Targets for Small Molecules: Principles, Progress, and Challenges. Pharmacol Rev *72*, 862-898.

Zhou, F., Yu, T., Du, R., Fan, G., Liu, Y., Liu, Z., Xiang, J., Wang, Y., Song, B., Gu, X*., et al.* (2020a). Clinical course and risk factors for mortality of adult inpatients with COVID-19 in Wuhan, China: a retrospective cohort study. Lancet *395*, 1054-1062.

Zhou, P., Yang, X.L., Wang, X.G., Hu, B., Zhang, L., Zhang, W., Si, H.R., Zhu, Y., Li, B., Huang, C.L*., et al.* (2020b). A pneumonia outbreak associated with a new coronavirus of probable bat origin. Nature *579*, 270-273.

Zhu, F.C., Guan, X.H., Li, Y.H., Huang, J.Y., Jiang, T., Hou, L.H., Li, J.X., Yang, B.F., Wang, L., Wang, W.J*., et al.* (2020). Immunogenicity and safety of a recombinant adenovirus type-5-vectored COVID-19 vaccine in healthy adults aged 18 years or older: a randomised, double-blind, placebo-controlled, phase 2 trial. Lancet *396*, 479-488.

Ziegler, C.G.K., Allon, S.J., Nyquist, S.K., Mbano, I.M., Miao, V.N., Tzouanas, C.N., Cao, Y., Yousif, A.S., Bals, J., Hauser, B.M.*, et al.* (2020). SARS-CoV-2 Receptor ACE2 Is an Interferon-Stimulated Gene in Human Airway Epithelial Cells and Is Detected in Specific Cell Subsets across Tissues. Cell *181*, 1016-1035 e1019.

Zost, S.J., Gilchuk, P., Case, J.B., Binshtein, E., Chen, R.E., Nkolola, J.P., Schafer, A., Reidy, J.X., Trivette, A., Nargi, R.S.*, et al.* (2020). Potently neutralizing and protective human antibodies against SARS-CoV-2. Nature *584*, 443-449.

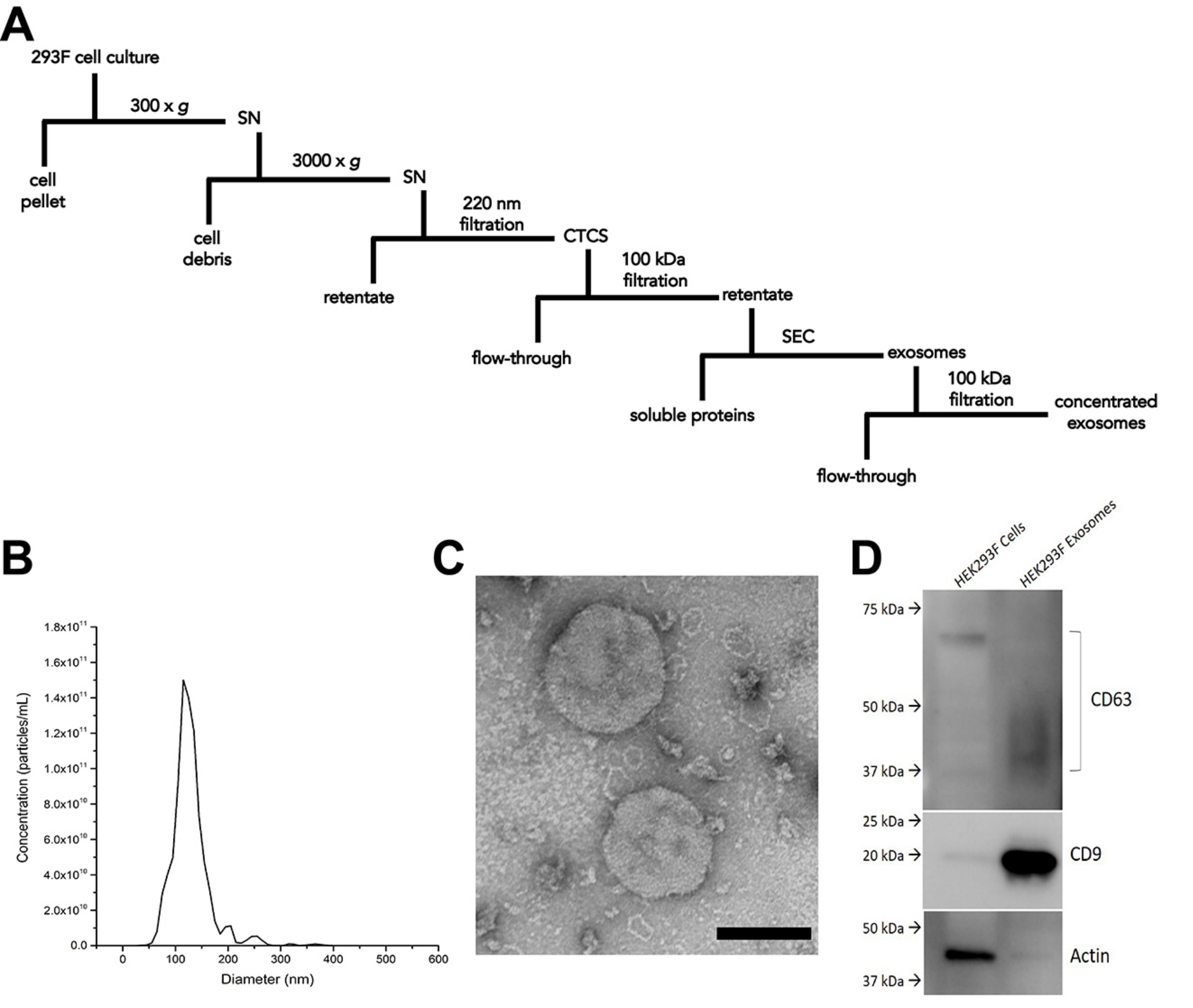
A
293F cell culture
300 x g
SN
cell pellet
3000 x g
SN
cell debris
220 nm filtration
CTCS
retentate
100 kDa filtration
retentate
flow-through
SEC
exosomes
soluble proteins
100 kDa filtration
concentrated exosomes
flow-through
B
Concentration (particles/mL)
Diameter (nm)
C
D
HEK293F Cells
HEK293F Exosomes
75 kDa
50 kDa
37 kDa
CD63
25 kDa
20 kDa
CD9
50 kDa
37 kDa
Actin

Figure 1

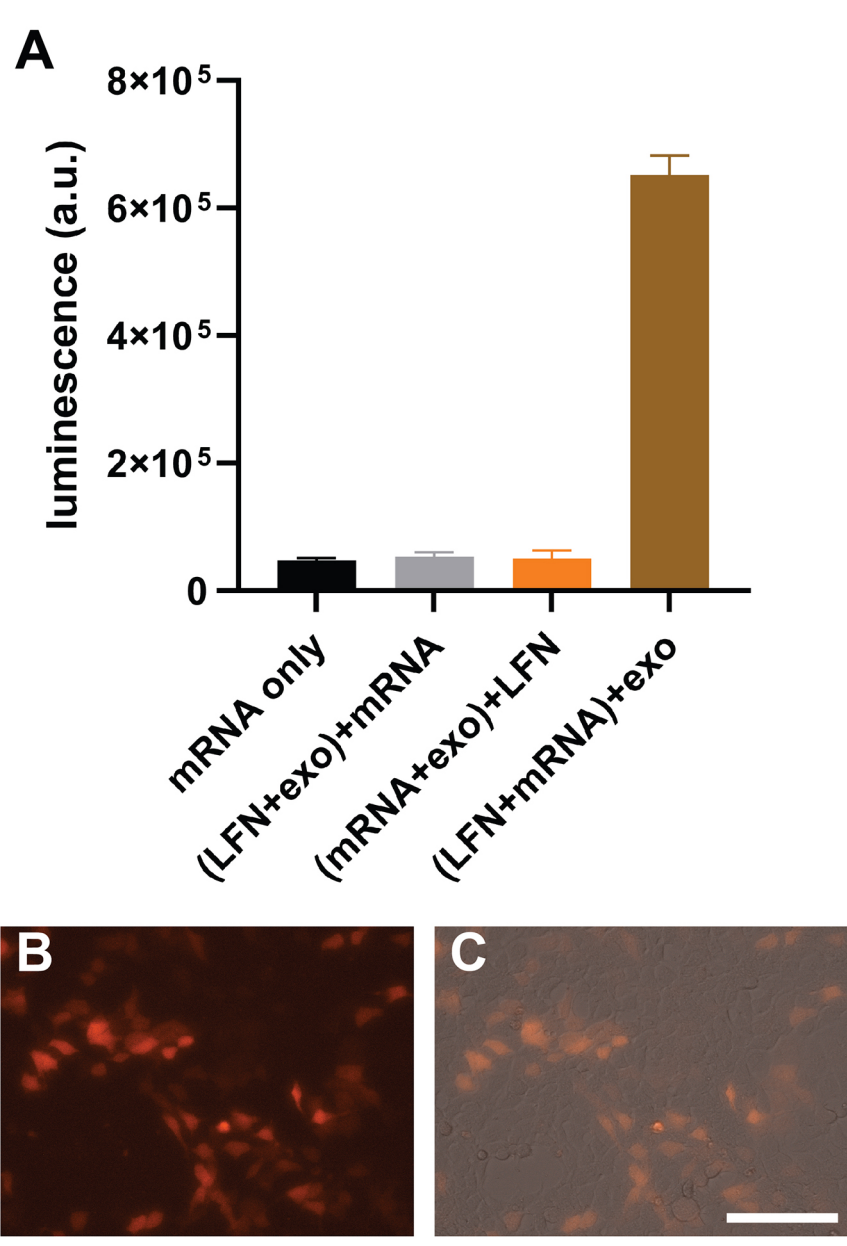
A
luminescence (a.u.)
8×10⁵
6×10⁵
4×10⁵
2×10⁵
0
mRNA only
(LFN+exo)+mRNA
(mRNA+exo)+LFN
(LFN+mRNA)+exo
B
C

Figure 2

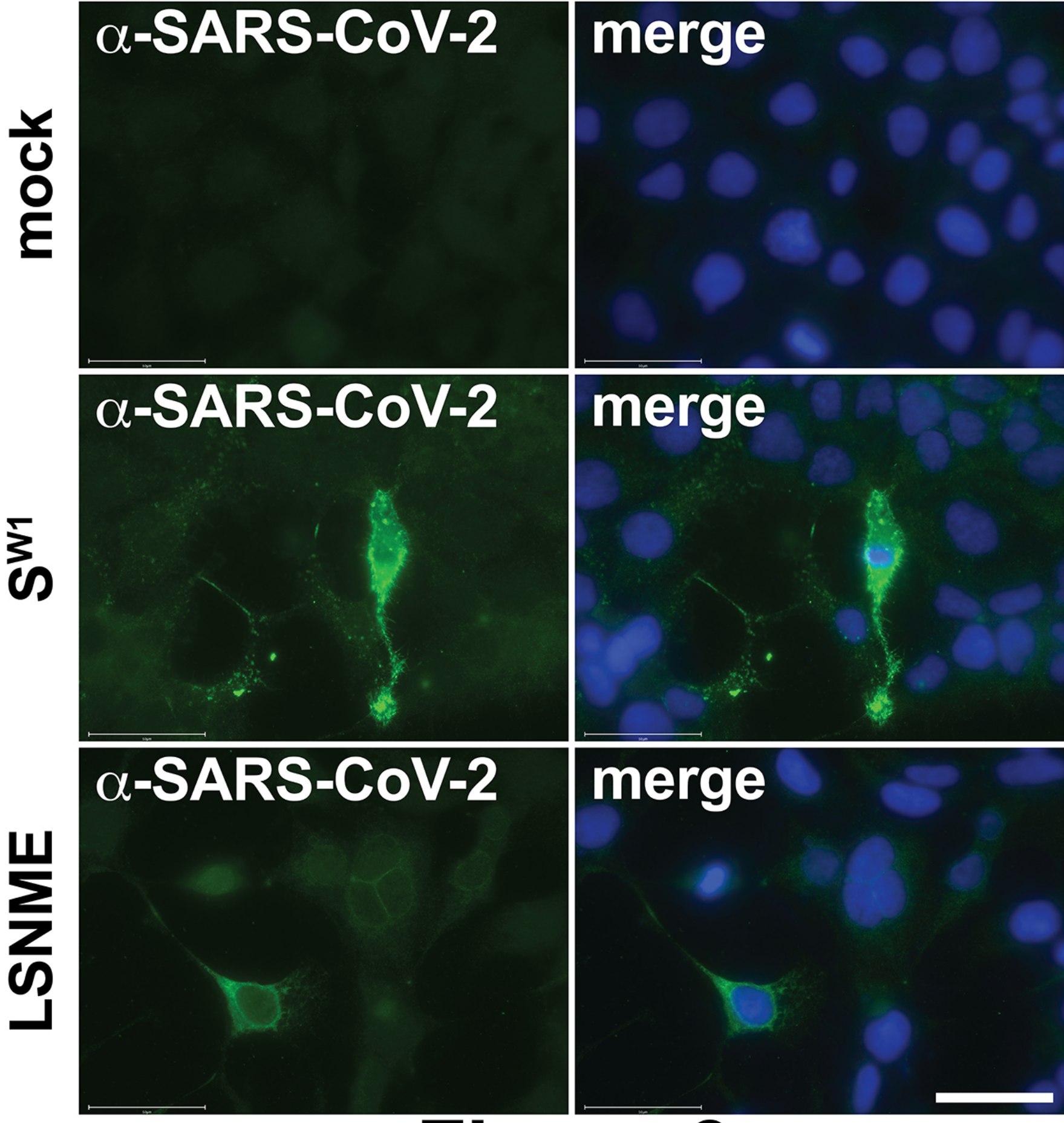
mock
SW1
LSNME
α-SARS-CoV-2
merge
α-SARS-CoV-2
merge
α-SARS-CoV-2
merge

Figure 3

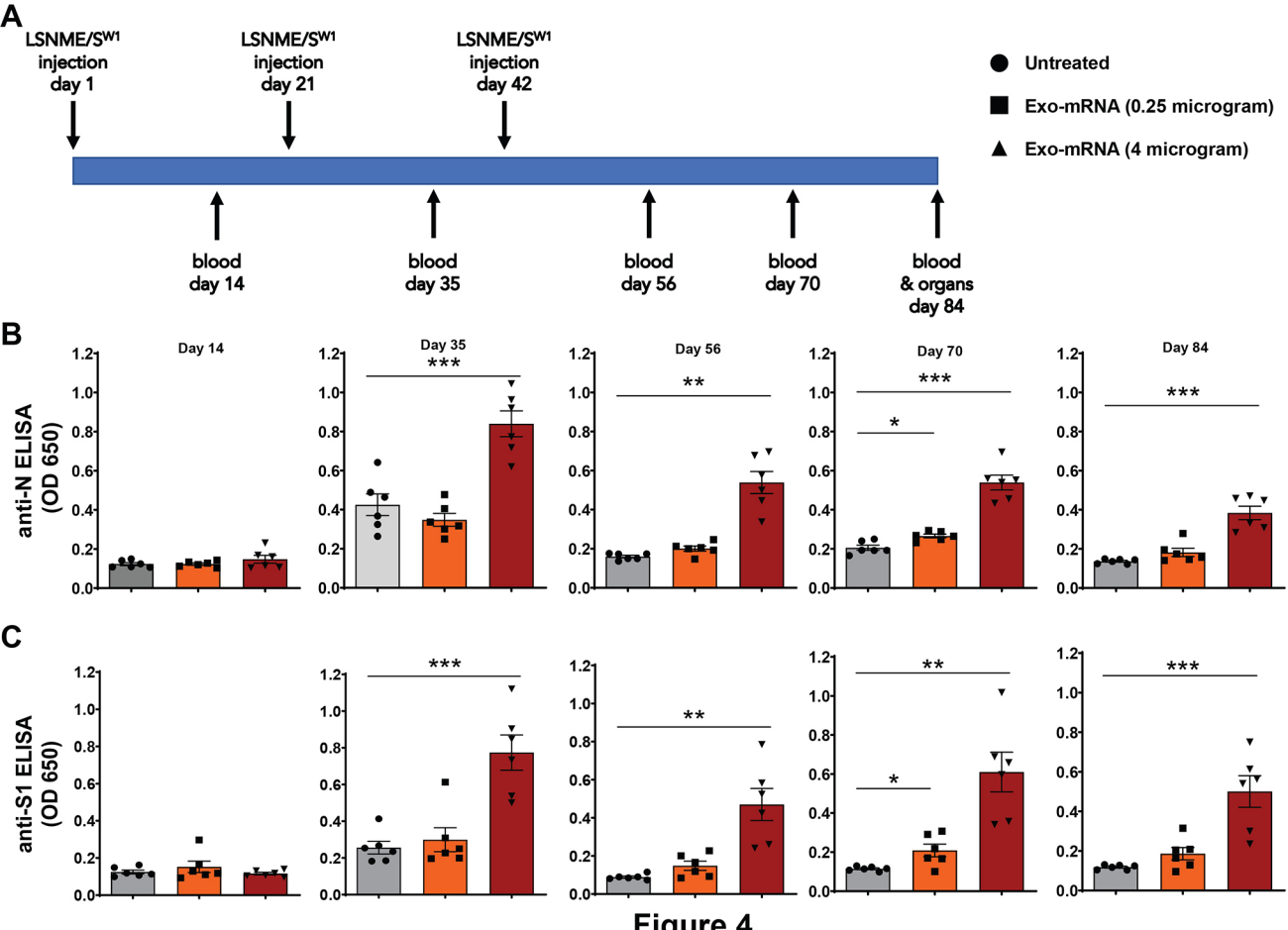
A
LSNME/SW1 injection day 1
LSNME/SW1 injection day 21
LSNME/SW1 injection day 42
Untreated
Exo-mRNA (0.25 microgram)
Exo-mRNA (4 microgram)
blood day 14
blood day 35
blood day 56
blood day 70
blood & organs day 84
B
anti-N ELISA (OD 650)
Day 14
Day 35
Day 56
Day 70
Day 84
C
anti-S1 ELISA (OD 650)

Figure 4

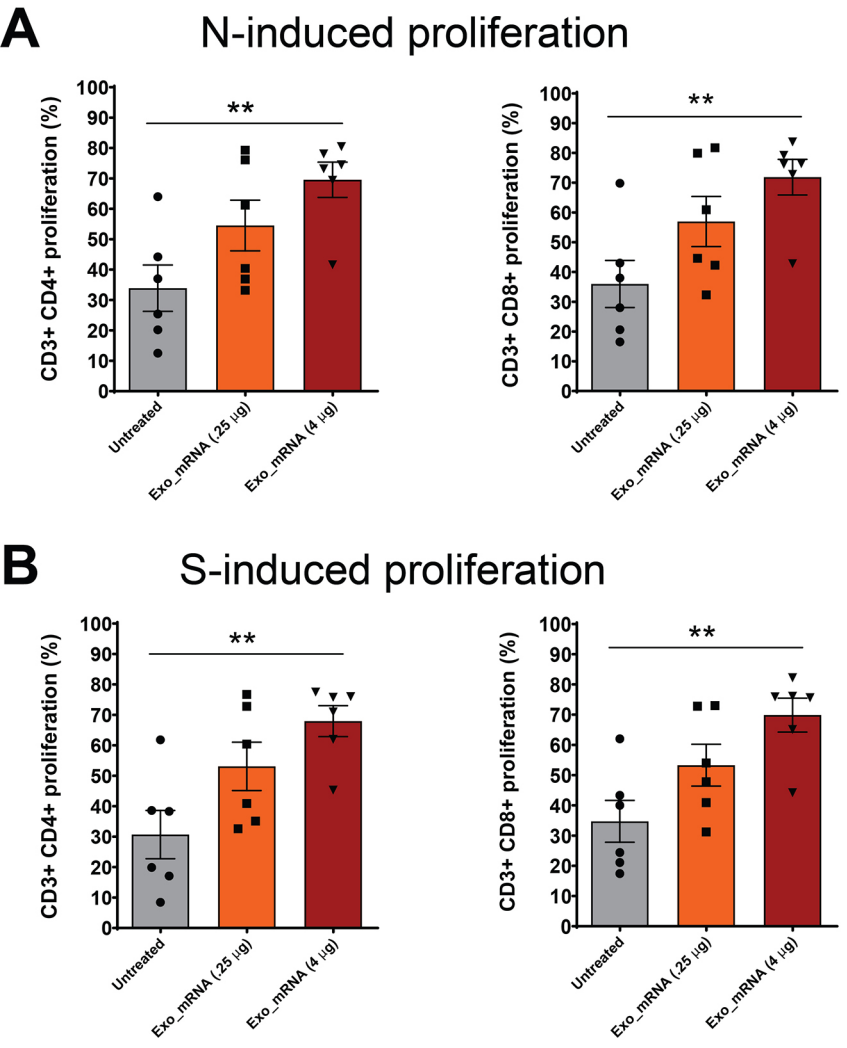
A
N-induced proliferation
CD3+ CD4+ proliferation (%)
CD3+ CD8+ proliferation (%)
**
Untreated
Exo_mRNA (.25 µg)
Exo_mRNA (4 µg)
B
S-induced proliferation
CD3+ CD4+ proliferation (%)
CD3+ CD8+ proliferation (%)
**
Untreated
Exo_mRNA (.25 µg)
Exo_mRNA (4 µg)

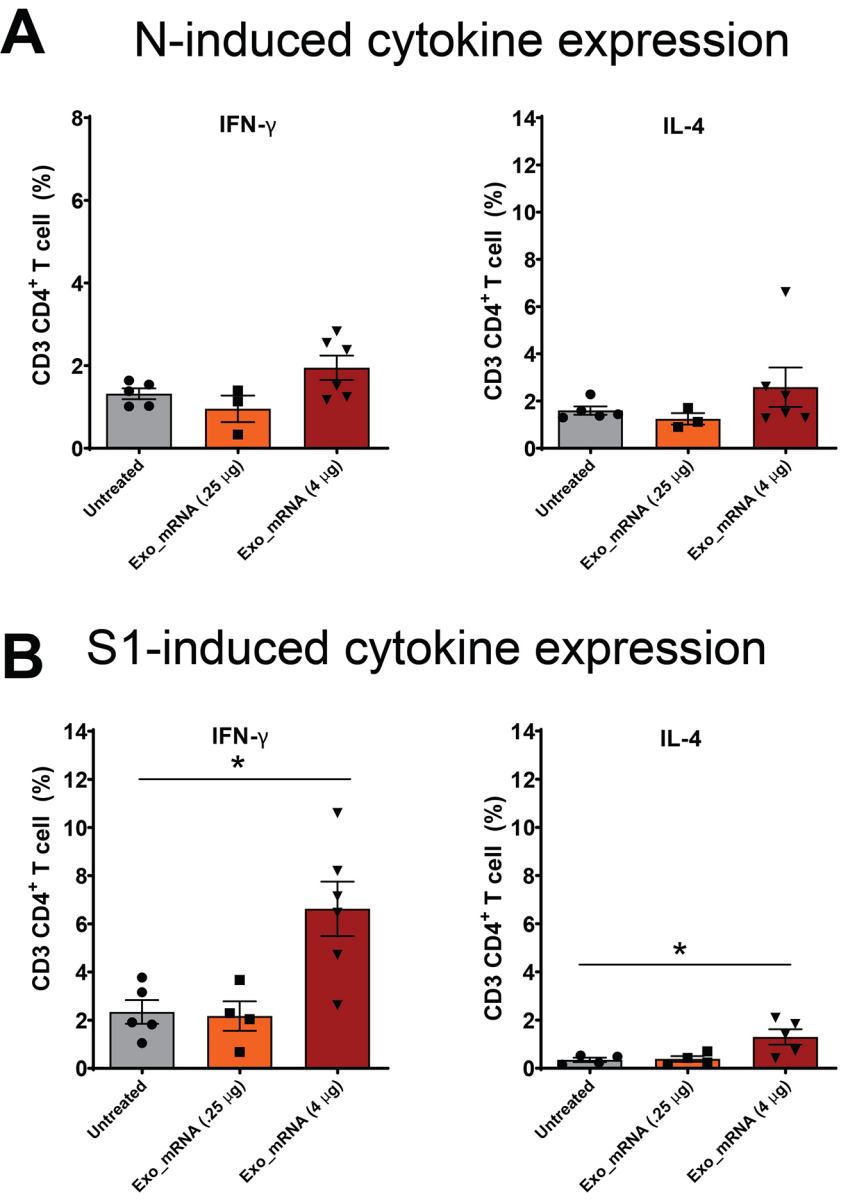
A
N-induced cytokine expression
IFN-γ
IL-4
CD3 CD4+ T cell (%)
Untreated
Exo_mRNA (25 μg)
Exo_mRNA (4 μg)
B
S1-induced cytokine expression
IFN-γ
IL-4
*
*

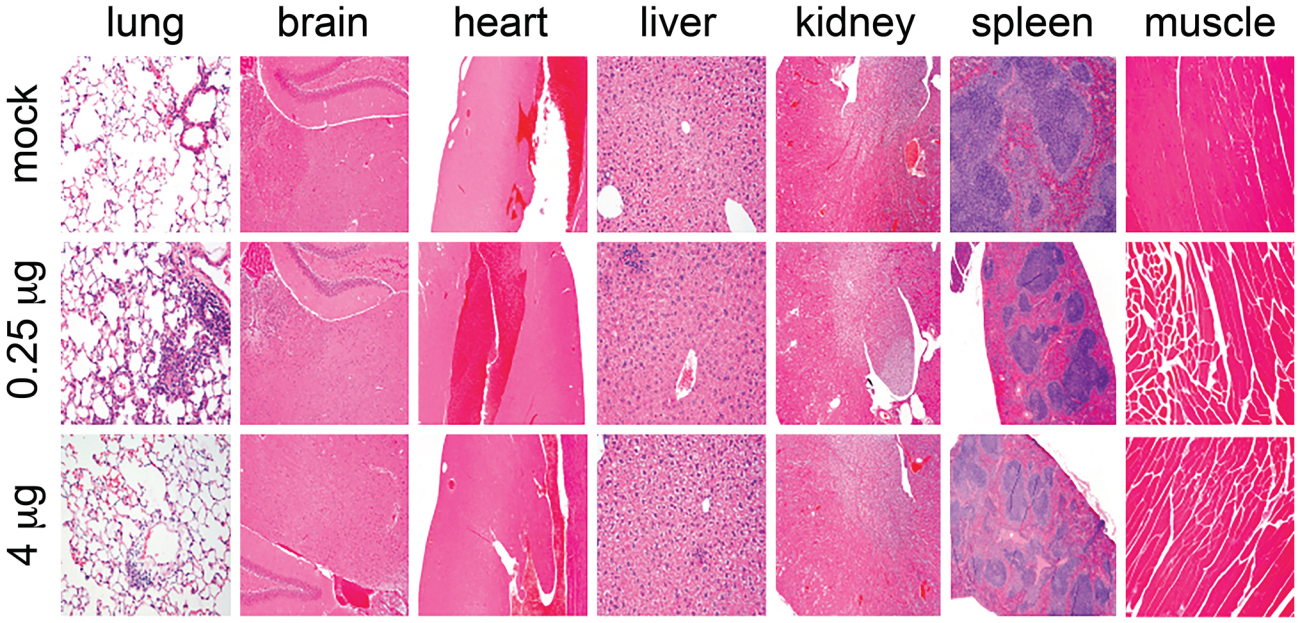

Figure 7

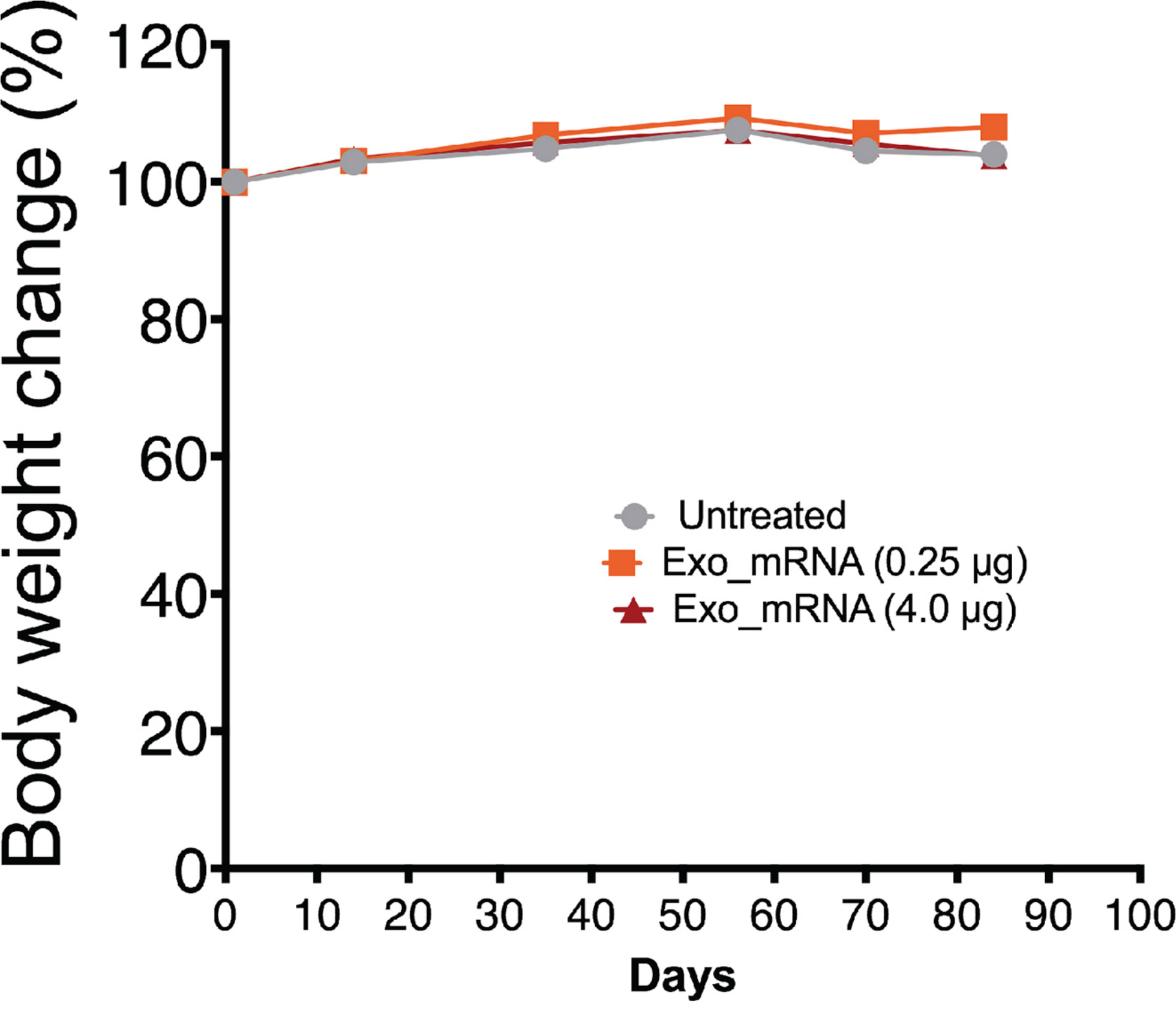

Supplemental Figure 1

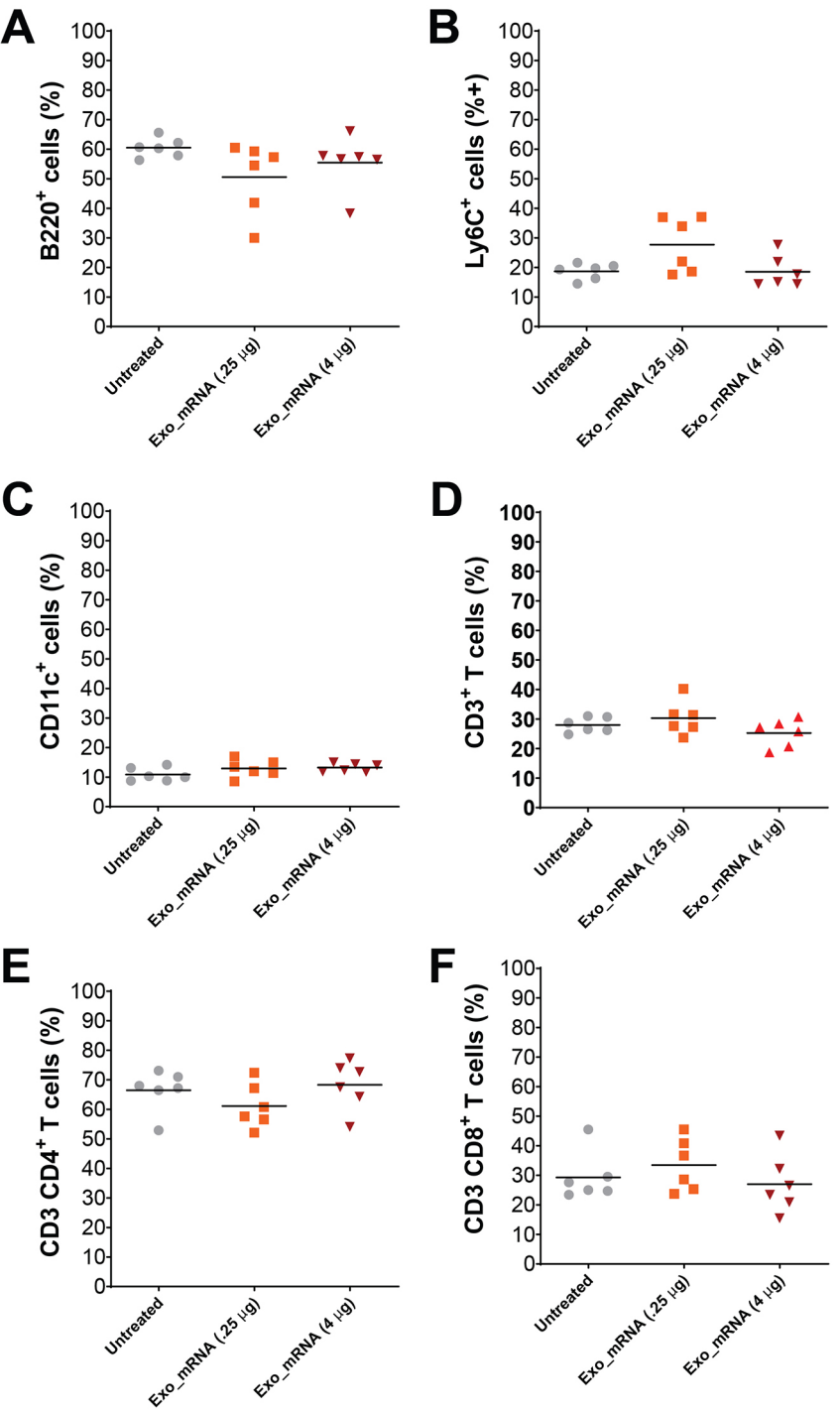

Supplemental Figure 2